Thin Solid Films 520 (2012) 1740–1744

Contents lists available at SciVerse ScienceDirect

Thin Solid Films

journal homepage: www.elsevier.com/locate/tsf

Applicability of X-ray fluorescence spectroscopy as method to determine thickness and composition of stacks of metal thin films: A comparison with imaging and profilometry

J.A.M. Vrielink [a,*,1], R.M. Tiggelaar [b,1], J.G.E. Gardeniers [b], L. Lefferts [a]

[a] Catalytic Processes and Materials, MESA+ Institute for Nanotechnology, University of Twente, P.O. Box 217, 7500 AE Enschede, The Netherlands
[b] Mesoscale Chemical Systems, MESA+ Institute for Nanotechnology, University of Twente, P.O. Box 217, 7500 AE Enschede, The Netherlands

ARTICLE INFO

Article history:
Received 3 March 2011
Received in revised form 8 August 2011
Accepted 15 August 2011
Available online 22 August 2011

Keywords:
X-ray fluorescence
Thickness
Non-destructive
Scanning electron microscopy
Profilometry
Metal thin films
Density

ABSTRACT

In this work the applicability of X-ray fluorescence spectroscopy (XRF) for fast, accurate and non-destructive determination of the thickness of a variety of single-layer and multi-layer metal thin films deposited on glass and silicon is investigated. Data obtained with XRF is compared with information from profilometry and images from scanning electron microscopy (SEM). Whereas thickness determinations based on profilometry and cross-sectional SEM-imaging have restrictions with respect to thickness of metal stacks or hardness of the metals, XRF has no such limitations. Moreover, XRF can discriminate between sublayers in a multi-layer film, and can also be utilized for compositional analysis and density estimations. Good agreement between thickness data obtained with XRF, profilometry and SEM-images is found, under the justifiable assumption that the density of sputter-deposited and evaporated thin films is ca. 5% below that of bulk metals. Similar XRF-results are found for non-patterned areas (64 mm^2 metal) as well as lithographically patterned areas containing a series of small metal lines (total metal surface ca. 8 mm^2). As a consequence, it is concluded that XRF is a versatile technique for analysis, verification, control or evaluation of the thickness, density or (elemental) composition of thin metal film line-patterns, during their fabrication as well as prior or post to applications.

© 2011 Elsevier B.V. All rights reserved.

1. Introduction

Since many decades X-ray fluorescence (XRF) spectroscopy has been used extensively for the quantitative analysis of specimens in terms of elemental composition, density or thickness [1,2]. XRF is commonly applied for precise analysis of geological materials (e.g. minerals, rocks), alloys, glass, cements, polymers and nowadays also for very thin film materials [3–9]. In fact, in the semiconductor industry XRF is an important in-line technique for quality and functional control during the manufacturing process of microelectronics [10]. Other typical applications of (patterned) thin metallic films and coatings are within the fields of catalysis [11,12] and microsystems technology: in micromachined devices of silicon and/or glass thin films can be used as heaters, temperature sensors, thermal actuators, electrodes or catalysts [13–17]. For such applications of (patterned) metallic thin films XRF is a powerful and fast analysis technique, as will be shown in this work.

Besides that XRF is a relatively fast, accurate and non physical-contact method, the main advantage with respect to other characterization techniques is its non-destructive character. Most other analysis techniques that can be used to determine the thickness, density and/or composition of metallic thin films do not meet all of the above-mentioned advantages, or are complex and therefore time-consuming. For example, cross-sectional scanning electron microscopy (SEM) requires cleavage of a specimen (destructive), and profilometry uses physical contact of a probe to a specimen with a thin film pattern. The mechanical contact in profilometry may damage the layers, furthermore discrimination between sublayers of a multi-layer thin film stack is difficult. The latter may be solved by combining profilometry with secondary ion mass spectrometry [9]. A well-approved non-contact method for thickness or density determination of thin films is X-ray reflectrometry (XRR), which also yields information on surface or interface roughness [9,10,18]. In case of determination of the thickness of single-element films in the range of a few to a few hundred nanometers, XRR has an uncertainty of ca. 1%. However, for multi-component single-layer and multi-layer films the uncertainty in the thickness estimation of the (sub)layer(s) increases significantly (up to 10%) [9,10], which restricts the use of XRR to films with a relatively simple composition as well as a limited thickness, i.e. films with not too many elements and/or sublayers, and with a total thickness in the range 10–100 nm [18]. X-ray fluorescence spectroscopy does not face these restrictions [19], and is therefore often used for quantitative analysis of solid thin films.

* Corresponding author. Tel.: +31 534892908; fax: +31 534894683.
E-mail address: j.a.m.vrielink@utwente.nl (J.A.M. Vrielink).
[1] Contributed equally to this work.

0040-6090/$ – see front matter © 2011 Elsevier B.V. All rights reserved.
doi:10.1016/j.tsf.2011.08.049

In this work the applicability of XRF for accurate, non-destructive determination of the thickness and composition of a variety of single-layer and multi-layer metal thin films deposited on glass and silicon is investigated. XRF-results are compared with data from profilometry and cross-sectional SEM-imaging. It is shown that XRF yields reliable data, and that XRF can be used for rapid, non-destructive control and verification of metallic thin film thickness and composition during and post to the fabrication process or application of such coatings.

2. Review of XRF theory

Although XRF is an important technique for thickness or density analysis of materials, the fundamental principles are not often described. Since this is crucial to understand the benefits of XRF with respect to other analysis methods, below a concise overview is given.

When a specimen is irradiated with high-energy primary X-ray photons, particles such as X-ray photons and electrons with sufficient energy are expelled/ejected from the atoms. This creates a 'hole' in (at least) one shell, resulting in the conversion of the atom into an unstable ion. In order to restore a (more) stable state, the holes (or 'initial vacancies') in inner shells are filled by transferring electrons from outer orbitals. Since outer shells have a higher energy than inner shells, such electron transitions are accompanied by energy emission in the form of secondary X-ray photons, which is referred to as fluorescence (Fig. 1).

The radiated energy of an electron depends on the shell it occupies (i.e. K, L, M-shells) as well as on the atom to which it belongs, which makes the measured emission spectrum unique for each element [20]. The intensity of each line in a fluorescence spectrum is related to the concentration of an element. However, fluorescent count rates are influenced by all (other) elements present in a specimen, manifested in so-called matrix effects. In case of a thin film specimen composed of more than one element, depending on its configuration (viz. a single or a multi-layered sample) absorption, enhancement and scattering effects within each layer, between layers and between layers and substrate can influence the characteristic radiation [20,21].

With XRF the thickness and/or composition of a specimen is determined by means of iterative matching of theoretical intensities and measured intensities (which are corrected for instrument responses) [22]. For this XRF utilizes mathematical calculations/equations that describe the process of X-ray generation in a specimen, and in these theoretical intensity calculations the elements and/or expected thickness(es) of the (sub)layer(s), as well as inter-element and inter-layer X-ray absorption and enhancements effects (a complicated process) have to be taken into account (details on the mathematics of XRF and parameter matching algorithms are not the goal of this work, and can be found in e.g. [20,23]). Two general models are developed to make these matrix corrections, i.e. the empirical coefficient (EC) method (also referred to a direct method or theoretical influence method) and the fundamental parameter (FP) method. Although both methods require compound standards, the FP-method has a relatively low demand for these standards (due to its iterative calculations), as a consequence of which the FP-method is more accurate and therefore mostly used for XRF-analysis [1,19,22,24]. The FP-method is based on the equation of Sherman, who in the 1950s derived a mathematical equation that describes the relation between intensity of an element and the composition of a specimen. It includes many physical constants and parameters (fundamental parameter), and based on X-rays physics matrix-effect corrections are calculated [20]. Nowadays the complex equations describing the matrix-effect corrections by the FP-method are solved by computers, which, in combination with the physical parameter calculations of de Boer [25], has given an enormous boost to FP-based XRF analysis since the late 1970s [26]. Since then many developments, refinements and optimizations of mathematical procedures, iteration and software criteria used in/for the FP-method have been reported, with the aim to make XRF-analysis more reliable, precise and accurate as well as to widen its applicability [2,27–32]. As a consequence, with FP-based XRF thickness and/or compositional analysis of single-, double- and triple-layer multi-component thin films can be accomplished with relative uncertainties in the range 1–10% [7–9,21,24,29,23]. The uncertainty in estimation of the (sub)layer thickness depends on the total thickness as well as the complexity of thin films. Due to technological advancements, throughout the years the lateral resolution of XRF was reduced from a few square centimeters to a few square millimeters. Recent developments in X-ray optics, i.e. the use of total reflection to focus X-rays, have resulted in spot sizes down to the range of tens of micrometers. This so-called micro-XRF makes it possible to perform analyses other than the classical thickness, density and/or composition, such as homogeneity verification (i.e. distribution of the components in a layer) [33,34], or in-line metrology [22].

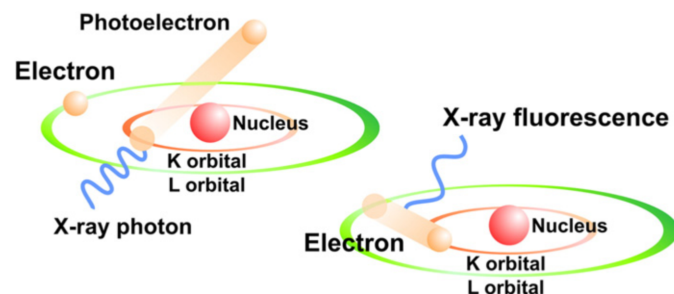

Fig. 1. Production of X-ray fluorescence.
Courtesy of Panalytical B.V., The Netherlands.

3. Experimental details

3.1. Preparation of metal thin films samples

Metal thin films were deposited on silicon substrates ((100)-oriented, p-type, resistivity 5–10 Ω cm, 100 mm diameter, thickness 525 μm, single side polished, roughness as-fabricated <1 nm; Okmetic, Finland) and fused silica substrates (UV Grade 7980F, diameter 100 mm, thickness 500 μm, roughness as-fabricated <1 nm; Corning, USA). Before thin film deposition, the substrates were ultrasonically cleaned in de-mineralized water (10 min), immersion in fuming 100% nitric acid for 10 min (Selectipur 100453, BASF), and boiling 69% nitric acid (VLSI 116445, BASF) for 15 min, followed by rinsing in de-mineralized water and dry spinning. After this cleaning sequence, on several silicon substrates a layer of 250 nm silicon dioxide (SiO_2) was grown using steam oxidation (1100 °C), and on other silicon substrates a layer of 30 nm or 75 nm silicon nitride (Si_3N_4) was deposited using low pressure chemical vapor deposition. In order to avoid damaging of the metal thin films at locations where the substrates are cleaved during dicing ('chipping'), prior to metal deposition squares of 8 mm × 8 mm were defined in spin-coated photoresist (Olin 907-12). This photoresist was used in a lift-off procedure (see below).

Deposition of metal thin films with a thickness in the range 35–260 nm was done *via* evaporation and sputtering. By means of evaporation on a Balzers BAK600 electron-gun evaporation system at pressures below 10^{-5} Pa, layers of gold (Au), chromium (Cr), nickel (Ni), palladium (Pd), platinum (Pt), tantalum (Ta) and/or titanium (Ti) were deposited. The purity of Ti and Ta was at least 99.95%, of other evaporated metals the purity was ≥99.99%. Sputter-deposition at room temperature (argon pressure 0.67 Pa; Ar purity 99.999%) was done on a home-built DC-magnetron sputtering system, having 3 sputter guns and 2-inch targets. Sputtered metals were gold (Au), chromium (Cr), rhodium (Rh), tantalum (Ta), titanium (Ti) and titanium–tungsten

(TiW). All sputter targets have a purity of 99.999%, except TiW (>99.9%). Single-layer, double-layer and triple-layer metal thin film configurations were made, of which an overview is given in the left part of Table 1.

After metal deposition, an ultrasonic resist lift-off step in acetone (>20 min; VLSI, 100038, BASF) was carried out, followed by immersion in isopropanol (10 min; VLSI 107038, BASF), rinsing in demineralized water (10 min) and dry spinning. Finally, the metal-coated substrates were diced into samples of 1 cm × 1 cm (Disco DAD-321 dicing machine).

3.2. Characterization of metal thin films samples

The total thickness of deposited metal thin film coatings was determined with profilometry (Veeco Dektak 8), high-resolution scanning electron microscopy (HR-SEM; Jeol LEO 1550 — this required manual cleavage of samples), and X-ray fluorescence spectroscopy (XRF; Philips PW 1480, including FPMulti-software from Panalytical B. V.). Prior to measurements on thin film samples the profilometer was calibrated using specimen with a defined thickness (supplied by Veeco). In case of HR-SEM imaging, for thin film thickness determination low inspection angles were used, i.e. the deviation from perpendicular cross-sectional observation was below 5°. The accelerating voltage was 1.2 kV. Pure metals were used as standards for XRF. For XRF no special treatment of thin film samples was required. In order to obtain a good counting statistic error, counting times of 998 s (at peaks) and 200 s (at backgrounds) were used. Further details of the spectrometer and used settings are given in Table 2. For each metal thin film coating shown in Table 1, XRF-analysis was performed once. Multiple thickness determinations (i.e. ≥3) were done using SEM-imaging and profilometry, of which the average thickness values are given in Table 1. All thickness data points based on SEM-imaging or profilometry were within 2.3% (SEM-imaging) and 3.8% (profilometry) of their average values, respectively. It is noted that in case of thicknesses below 50 nm the instrumental error of the height-profiling system (±5 nm) dominates the deviation of profilometry.

4. Results and discussion

In Table 1 the thickness values for the deposited metal films, as determined with profilometry, cross-sectional SEM-imaging and XRF, are shown. Only XRF can discriminate sublayers of a stack, and no noticeable differences in estimations of the thicknesses of sputtered and evaporated thin films are found.

Table 2
Spectrometer settings.

Element	Line	Crystal	2Θ (peak)	2Θ (background)	kV/mA	Collimator	Detector
Au	Lα	LIF200	37.020	1.5	50/50	Fine	FS
Cr	Kα	LIF200 (F)	69.47	1.5	50/50	Fine	FL
Ni	Kα	LIF200	48.745	3.0	50/50	Fine	FS
Pd	Kα	LIF200	16.805	−1/+2	60/40	Fine	SC
Pt	Lα	LIF200	38.125	−3/+2	50/50	Fine	FS
Rh	Kα	LIF200	17.595	−1/+1.5	60/40	Fine	SC
Ta	Lα	LIF200	44.490	2.0	50/50	Fine	FS
Ti	Kα	LIF200	86.260	6.0	50/50	Fine	FL
W	Lα	LIF200	43.095	−3.0	50/50	Fine	FS

LIF200: lithium fluoride, FL: flow counter, SC: scintillation counter, FS: combined FL and SC counter. (F): use of Al filter. Other information PW 1480 system: Cr tube anode, take-off angle 26°, sample geometry 61°/40°, Be-window mass thickness 0.0925 g/cm.

Profilometry and XRF data demonstrate good agreement. Fig. 2 shows the correlation between the layer thickness obtained by profilometry and XRF: a linear trend line that passes the origin has a slope of 1.06 and a correlation coefficient of 0.9896.

This shows that XRF, assuming that the profilometry data are correct, underestimates the thickness of metal thin films by ca. 6%. In the worst case the deviation between profilometry and XRF is 10%, which occurs for a layer thickness below 50 nm (Fig. 2), where the instrumental error of the height-profiling system of ±5 nm becomes dominant.

From Table 1 it can be seen that for the majority of the studied metal thin film samples there is good agreement between thickness values as determined by XRF and SEM-images. However, in some cases thickness data based on SEM-images deviates significantly from values found with profilometry and XRF. The soft nature of some of the metals prevented accurate thickness measurement, because cleaving of films of these metals results in damage to the metal stack, with the consequence that no useful cross-sectional SEM-images can be made. This problem is particularly severe for Au-containing stacks, but also for stacks containing Pd or Pt this is an issue. In Fig. 3 the cross-section of a non-damaged Ni/Ta stack is shown, as well as a Pt/Au/Ti stack that suffered from severe deformation.

When thickness data of samples containing Au, Pt or Pd as obtained by HR-SEM and XRF are omitted from a correlation graph, the slope of the trend line passing the origin is 1.03 with a correlation coefficient of 0.9998 (Fig. 4; substrates 1, 9–11, 13–15 are not included). Thus, for metals that do not deform during cleavage,

Table 1
Details of prepared metal thin films, and layer thickness as determined with profilometry, cross-sectional SEM-imaging and X-ray fluorescence spectroscopy (note: sublayer "part I" is deposited after sublayer "part II" etc.).

Substrate			Metal thin film coating		Thickness of metal thin film [nm]					
I. D.	Material	Dielectric layer	Deposition method	Layer(s) (I/II/III)	Profilometry	SEM-imaging	XRF (total)	XRF (sublayers)		
								Part I	Part II	Part III
1	Fused silica	–	Sputtering	Au/Cr	109.3	n.a.	106	100.1	5.9	–
2	Silicon	SiO_2	Sputtering	Ta	143.2	143.5	139.5	139.5	–	–
3	Silicon	SiO_2	Sputtering	Ta	22.6	18.8	17.4	17.4	–	–
4	Silicon	SiO_2	Sputtering	Ta	73.5	72.6	69.7	69.7	–	–
5	Silicon	SiO_2	Sputtering	Rh/Ta	66.2	62.4	60.1	46.1	14	–
6	Silicon	SiO_2	Sputtering	Rh/TiW	39.3	31.9	30.9	21	9.9	–
7	Silicon	Si_3N_4	Sputtering	Rh/Ta	67.1	62.1	59.4	45.5	13.9	–
8	Silicon	Si_3N_4	Sputtering	Rh/TiW	38.9	32.2	31	21.1	9.9	–
9	Silicon	Si_3N_4	Sputtering	Pt/Au/Ti	245.8	192.2	232	176.4	47.9	7.7
10	Silicon	SiO_2	Evaporation	Pd/Ti	63.4	61.8	66.3	55.2	11.1	–
11	Silicon	SiO_2	Evaporation	Pt/Ta	51.2	46.7	41.1	30.9	10.2	–
12	Silicon	SiO_2	Evaporation	Ni/Ta	26.9	26.7	25.4	18.4	7	–
13	Silicon	SiO_2	Evaporation	Au/Cr	86.3	n.a.	73.4	66.6	6.8	–
14	Silicon	Si_3N_4	Evaporation	Pd/Ti	63.6	62.3	68.4	56.8	11.6	–
15	Silicon	Si_3N_4	Evaporation	Pt/Ta	52.6	47.1	41.6	31.2	10.4	–
16	Silicon	Si_3N_4	Evaporation	Ni/Ta	27.9	26.4	25.2	18.2	7	–

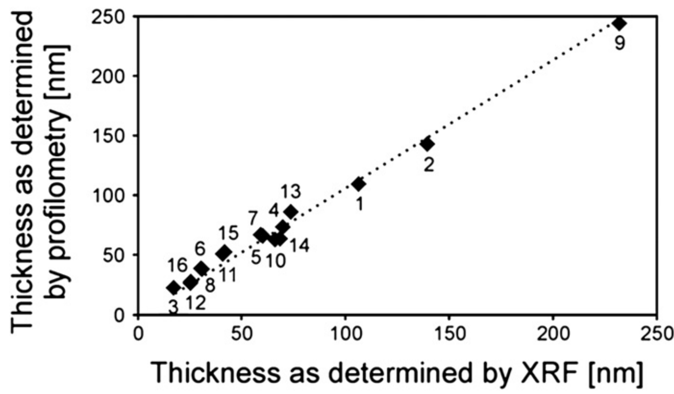

Fig. 2. Correlation of thickness values determined by profilometry and XRF (numbers represent substrate IDs as described in Table 1).

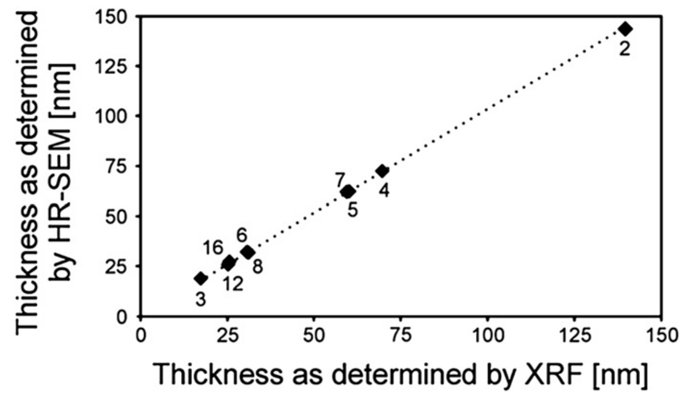

Fig. 4. Correlation of thickness values determined by HR-SEM and XRF (numbers represent substrate IDs as described in Table 1).

estimations of their thickness by means of HR-SEM and XRF highly match.

XRF-analysis software (FPMulti) uses the density of metals as input parameter to estimate the thickness of films, for which usually bulk values are taken. However, it is known that metal thin films might have a lower density than bulk metals [9,35], for example 50 nm FeNi has a density of 94% of the bulk value [19]. In case of sputter-deposition lower densities are caused by the inclusion of argon in the thin films, however, for evaporation a distinct reason for such density deviations is not known. Since XRF is based on mass-thickness analysis (rather than geometrical-thickness analyses, as most methods mentioned in section 2), comparison-and-matching of thickness-data obtained by XRF and other analysis techniques offers a way to estimate the density of thin films. By adapting density values in the software, the estimations of the thickness of films composed of Ni, Rh, Ta and/or TiW as determined by XRF, HR-SEM and profilometry correspond even better, to within 2–5%, when the densities of Ni, Rh, Ta and TiW are taken 4.7%, 4.7%, 4.1% and 5.0% lower than the respective bulk values. These percentages highly coincide with previously reported values, as a consequence of which it is concluded that the density of evaporated and sputtered thin films used in this work is ca. 5% lower than the bulk density.

All the above-mentioned XRF-results are obtained on metallic surfaces of 8×8 mm, thus 64 mm^2. On samples that contain a collection of small metal lines (25–200 μm in width, 1.5 mm long) within this analysis area, i.e. a smaller amount of metal-surface (7.5 mm^2), similar results are found in terms of thickness of films (compared to analysis areas that are 100% covered with metal). Only for films with a thickness below ca. 30 nm (i.e. substrates 2, 12 and 16) differences in sensitivity/resolution are found between line-patterned and non-patterned samples, which is due to the limited amount of metal present in case of line-patterned samples resulting in a low amount of counts.

Thus, provided that the metal layer is sufficiently thick (>30 nm) and that at least ~12% of an analysis-area of 8×8 mm is covered with metal, the thickness, density or composition of thin film metallic coatings can be determined with the used XRF-settings. These limits on layer thickness and area-coverage can be upgraded by using longer counting times. Such small amounts of metal-surface (7.5 mm^2) allow the use of conventional XRF for analysis, verification, control or evaluation of the thickness, density or composition of thin metal film structures (e.g. line-patterns) in microsystems, during fabrication as well as prior or post to applications and experiments.

5. Conclusions

In this work the applicability of XRF for fast, accurate and non-destructive determination of the thickness of a variety of single-layer and multi-layer metal thin films deposited on glass and silicon is investigated. Data obtained with XRF is compared with information from profilometry and SEM-imaging. There is good agreement between the thickness-data obtained with XRF, SEM-imaging and profilometry, but XRF is the only method that can discriminate between sublayers in metal films. Moreover, whereas profilometry is found to be less reliable for layers thinner than 50 nm and (destructive) cleavage of films containing "soft" metals yields unreliable cross-sectional SEM-images, XRF does not face such limitations. Besides thickness analysis, XRF can also be utilized for compositional analysis and/or density estimations. For sputter-deposited and evaporated thin films used in this work, excellent agreement between the thickness as estimated based on XRF, profilometry and SEM is found when the density of the metals is assumed to be ca. 5% lower than bulk values. Since the analyzed metal-surface area is relatively small, XRF is a valuable technique for analysis, verification, control evaluation of the thickness, density and (elemental) composition of (lithographically patterned) thin metal

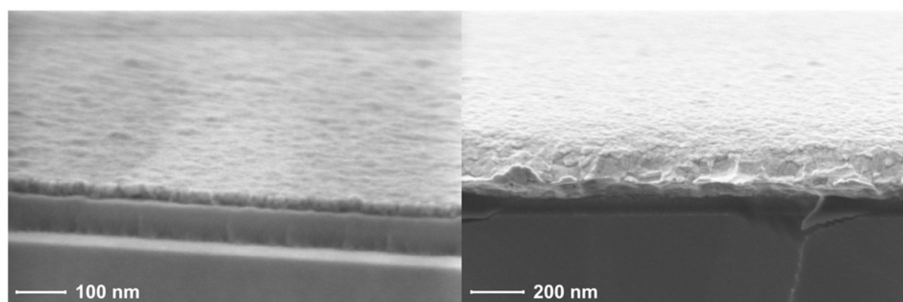

Fig. 3. Cross-sectional SEM-images of metal thin films: Ni/Ta (left) vs. Pt/Au/Ti (right).

film structures in micro-systems. Additionally, XRF is a fast and attractive method to verify or tune the deposition rates of metal deposition equipment.

Acknowledgments

The authors acknowledge Ties Bos, Peter Brouwer and Marco van der Haar for fruitful discussions and Mark Smithers for recording SEM-images.

References

[1] X.Y. Han, S.J. Zhuo, R.X. Shen, P.L. Wang, A. Ji, J. Quant. Spectrosc. Radiat. Transfer 97 (2006) 68.
[2] R. Sitko, Spectrochim. Acta B 64 (2009) 1161.
[3] K. Hirokawa, H. Gotô, Fresenius J. Anal. Chem. 185 (1962) 124.
[4] K. Hirokawa, T. Shimanuki, H. Gotô, Fresenius J. Anal. Chem. 190 (1962) 309.
[5] M. Bos, B.A. Boukamp, J.A.M. Vrielink, Anal. Chim. Acta 459 (2002) 305.
[6] T.C. Huang, J.K. Howard, Thin Solid Films 148 (1987) 209.
[7] S. Lehto, L. Niinistö, I. Yliruokanen, Fresenius J. Anal. Chem. 346 (1993) 608.
[8] M. Kolbe, B. Beckhoff, M. Krumrey, G. Ulm, Spectrochim. Acta B 60 (2005) 505.
[9] O. Baake, P.S. Hoffmann, S. Flege, H.M. Ortner, S. Gottschalk, W. Berky, A.G. Balogh, W. Ensinger, B. Beckhoff, M. Kolbe, M. Gerlach, B. Pollakowski, J. Weser, G. Ulm, M. Haschke, E. Blokhina, M. Peter, D. Porta, M. Heck, Anal. Bioanal. Chem. 393 (2009) 623.
[10] C. Wyon, D. Delille, J.P. Gonchond, F. Heider, L. Kwakman, S. Marthon, I. Mazor, A. Michallet, D. Muyard, L. Perino-Gallice, J.C. Royer, A. Tokar, Thin Solid Films 450 (2004) 84.
[11] J.K. Chinthaginjala, J.H. Bitter, L. Lefferts, Appl. Catal. A: Gen. 383 (2010) 24.
[12] S. Pacheco Benito, L. Lefferts, Carbon 48 (2010) 2862.
[13] R.M. Tiggelaar, J.W. Berenschot, J.H. de Boer, R.G.P. Sanders, J.G.E. Gardeniers, R.E. Oosterbroek, A. van den Berg, M.C. Elwenspoek, Lab Chip 5 (2005) 326.
[14] G. Fleury, C. Malhaire, C. Populaire, M. Verdier, A. Devos, P.-L. Charvet, J.-P. Polizzi, Sens. Actuators B 126 (2007) 48.
[15] M. Odijk, A. Baumann, W. Lohmann, F.T.G. van den Brink, W. Olthuis, U. Karst, A. van den Berg, Lab Chip 9 (2009) 1687.
[16] D.B. Thakur, R.M. Tiggelaar, T.M.C. Hoang, J.G.E. Gardeniers, L. Lefferts, K. Seshan, Appl. Catal. B: Environ. 102 (2011) 232.
[17] D.B. Thakur, R.M. Tiggelaar, Y. Weber, J.G.E. Gardeniers, L. Lefferts, K. Seshan, Appl. Catal. B: Environ. 102 (2011) 243.
[18] T.C. Huang, W.Y. Lee, Anal. Sci. 11 (1995) 529.
[19] T.C. Huang, X-ray Spectrom. 20 (1991) 29.
[20] P.N. Brouwer, in: B. Beckhoff, B. Kanngieβer, N. Langhoff, R. Wedell, H. Wolff (Eds.), Chapter 5 of “Handbook of practical X-ray fluorescence analysis”, Springer Verlag, Berlin, Germany, 2005.
[21] M. Mantler, Anal. Chim. Acta 188 (1986) 25.
[22] L.M. van der Haar, C. Sommer, M.G.M. Stoop, Thin Solid Films 450 (2004) 90.
[23] M.H.J. Bekkers, H.A. van Sprang, X-ray Spectrom. 26 (1997) 122.
[24] T.C. Huang, Thin Solid Films 157 (1988) 283.
[25] D.K.G. de Boer, Spectrochim. Acta B 44 (1989) 1171.
[26] D. Laguitton, W. Parrish, Anal. Chem. 49 (1977) 1152.
[27] M. Bos, J.A.M. Vrielink, Anal. Chim. Acta 373 (1998) 291.
[28] M. Bos, J.A.M. Vrielink, W.E. van der Linden, Anal. Chim. Acta 412 (2002) 203.
[29] K. Nygård, K. Hämäläinen, S. Manninen, P. Jalas, J.-P. Ruottinen, X-ray Spectrom. 33 (2004) 354.
[30] M. Bos, J.A.M. Vrielink, Anal. Chim. Acta 545 (2005) 92.
[31] S.P. Formica, S.M. Lee, Thin Solid Films 491 (2005) 71.
[32] R.M. Rousseau, Open Spectrosc. J. 3 (2009) 31.
[33] C. Vogt, R. Dargel, Appl. Surf. Sci. 252 (2005) 53.
[34] R. Dargel, M. Azeroual, B. Mogwitz, J. Janek, C. Vogt, J. Mater. Sci. 42 (2007) 7375.
[35] O. Baake, R.M. Öksüzoglu, S. Flege, P.S. Hoffmann, S. Gottschalk, H. Fuess, H.M. Ortner, Mater. Charact. 57 (2006) 12.